

First principal investigation of Structural optical
and thermoelectric properties of hybrid
organic-inorganic perovskite
 $[\text{NH}_3-(\text{CH}_2)_4-\text{NH}_3]\text{CdCl}_4$ compound

Hafida ZIOUANI¹, Sanaa MAZOUAR¹,
Jean-Pierre TCHAPET NJAFA^{2*}, Taoufik ABDELILAH¹,
Mahmoud ETTAKNI¹, El Mostafa KHECHOUBI¹

¹Department of Physics, Faculty of Science, Materials and Renewable Energy Team, LP2MS Laboratory, Moulay Ismail University, Meknes, Morocco.

^{2*}Department of Physics, Faculty of Science, University of Yaoundé 1, Yaoundé, 812, Cameroon.

*Corresponding author(s). E-mail(s):

jean-pierre.tchapet@facsciences-uy1.cm;

Contributing authors: ha.ziouani@edu.umi.ac.ma;

s.mazouar@edu.umi.ma; taoufik.abdelillah@edu.umi.ac.ma;

M.ETTAKNI@umi.ac.ma; khechoubi@umi.ac.ma;

Abstract

The structural, thermoelectric, and optical properties of $[\text{NH}_3-(\text{CH}_2)_4-\text{NH}_3]\text{CdCl}_4$ were studied using Density Functional Theory (DFT) within the ABINIT code. The GGA-PBE functional, plane wave pseudopotentials, a kinetic energy cutoff of **35 Ha**, and an 11x8x8 Monkhorst-Pack \mathbf{k} -point grid were employed. The material comprises inorganic $[\text{CdCl}_4]^{2-}$ sheets, organic $[\text{NH}_3-(\text{CH}_2)_4-\text{NH}_3]^{2+}$ layers, and N-H-Cl hydrogen bonds, ensuring sublattice cohesion. Structural optimization used reference crystal data, enabling analysis of alkylene-diammonium chain conformation, intermolecular interactions, and crystal stability. The study highlights the role of Cd in influencing optical and thermoelectric properties. Temperature-induced changes lead to a reduced band gap and enhanced optical absorption, indicating significant electronic structure modifications. These findings propose

$[\text{NH}_3-(\text{CH}_2)_4-\text{NH}_3]\text{CdCl}_4$ as a promising candidate for optoelectronic applications, particularly after thermal cycling, due to its improved performance under varying conditions.

Keywords: DFT-GGA, electronic properties, band gap, optical properties, solar cells

1 Introduction

Due to their numerous applications in technology and industry, perovskite compounds have been the subject of considerable interest among researchers. The structure of perovskite materials was first discovered in 1839 by Gustav Rose, and these materials exhibit a range of distinctive and exceptional physical properties, including ferromagnetism, spin-dependent transport, high T_c superconductivity, high thermopower, ferroelectricity, and so on.

Given their abundance in nature, low cost, and ease of deposition into thin films, organic-inorganic halide hybrid perovskites (ABX_3 : A = big organic cation, B = metal cation, and X = halogen anion) offer considerable potential for usage in commercial applications [1].

Thermoelectric materials are of universal interest due to their capacity to transform heat into electric energy, rendering them a significant source of energy [2, 3]. Currently, the world requires thermoelectric supplies to reduce its reliance on fossil fuels. Perovskite compounds exhibit exceptional thermoelectric properties, which have prompted the development of thermoelectric device appliances. In the field of high-temperature thermoelectric research, germanium-based chloro perovskites have garnered significant attention in recent years [4]. Lead is a toxic substance for the environment, whereas hybrid perovskite is a free material and therefore environmentally benign. Consequently, it can be employed in photovoltaic applications with minimal environmental impact.

The crystal structure of $[\text{NH}_3-(\text{CH}_2)_4-\text{NH}_3]\text{CdCl}_4$ is composed of an infinite number of inorganic layers. Each layer is formed by corner-sharing CdCl_6 octahedra, arranged in a two-dimensional perovskite-like structure. The alkyl ammonium (or alkylammonium) chains are oriented almost perpendicular to the planes of the layer. The NH_3 groups at the end of the organic chain engage in $\text{N}-\text{H}-\text{Cl}$ hydrogen bonds with the octahedra.

Previous studies have investigated thermal and crystallographic analyses [5]. Evidence of five crystalline forms, designated V, IV, III, II, and I, has been identified. It has been established that the various phase transitions are either irreversible or reversible. The various phase transitions of this complex can be associated with the conformational evolutions of the organic part $[\text{NH}_3-(\text{CH}_2)_4-\text{NH}_3]^{2+}$, thanks to structural determinations of the "limit" Phases five (**V**: the initial room-temperature form) and one (**I**: the new room-temperature form) [6]. A review of the literature reveals that an increase in temperature at **Phase V** results in an irreversible change from the "gauche" conformation of the organic chain to an "all-trans" conformation, with the final conformation retained during subsequent phase transitions. In addition

to these crystallographic studies, recent work has investigated the electronic and optical properties of similar hybrid perovskites, such as $[\text{NH}_3-(\text{CH}_2)_4-\text{NH}_3]\text{MX}_4$ ($\text{M} = \text{Cu}, \text{Mn}$), using Density Functional Theory (DFT) [7]. These studies have revealed that the substitution of Cu and Mn significantly alters the electronic and optical behaviors, making these compounds promising candidates for optoelectronic applications.

In this work, we will study the effect of Phase transitions, especially the **Phase V** and **I**, on the structural, electronic, optical, and thermoelectric properties of the compound $[\text{NH}_3-(\text{CH}_2)_4-\text{NH}_3]\text{CdCl}_4$.

2 Computational details

The Density Functional Theory+U (DFT+U) method implemented in the ABINIT code [8, 9] was utilized to investigate the structural and electronic properties of $[\text{NH}_3-(\text{CH}_2)_4-\text{NH}_3]\text{CdCl}_4$. The double counting correction known as Full localised limit (FLL) [10] was employed, along with the Generalised Gradient Approximation (GGA) in the Perdew-Burke-Ernzerhof functional [11]. The DFT+U method is an extension of the standard Density Functional Theory (DFT) approach that incorporates an additional correction for treating the electron-electron interactions within localized orbitals. The pseudopotential was generated using the Projector Augmented-Wave approach [12]. A cutoff of kinetic energy at 35 Ha was utilized to carry out self-consistent field (SCF) and non-self-consistent field (NSCF) calculations on $[\text{NH}_3-(\text{CH}_2)_4-\text{NH}_3]\text{CdCl}_4$. The Monkhorst Pack Mesh scheme adopted a k -points grid sampling of $11 \times 8 \times 8$ for conducting the integrations of the irreducible Brillouin zone of $[\text{NH}_3-(\text{CH}_2)_4-\text{NH}_3]\text{CdCl}_4$. The crystal data of $[\text{NH}_3-(\text{CH}_2)_4-\text{NH}_3]\text{CdCl}_4$, as reported in the literature [5], served as the initial reference point.

3 Results and discussion

3.1 Structural properties

After a geometry optimization, the fitting of Birch-Murnaghan equation of state [13, 14] results in optimized lattice parameters of $[\text{NH}_3-(\text{CH}_2)_4-\text{NH}_3]\text{CdCl}_4$ by the GGA-PBE approximation in the two Phases are presented in Figure 1 and table 1, which are in great agreement with previous experimental measurements findings [5], confirming the accuracy of the present simulation. More interestingly, all the properties treated in this work (electronic, optical, and thermoelectric properties) are calculated after the full structure relaxation, including lattice constants, atomic positions, and free total energies of supercells.

3.2 Electronic properties

The density of the state is one of the most important properties that gives information about the behavior and electronic character of this system. It also allows knowing the nature of the chemical bonds between atoms. The total (TDOS) and partial (PDOS) densities of states are calculated at their equilibrium states by the

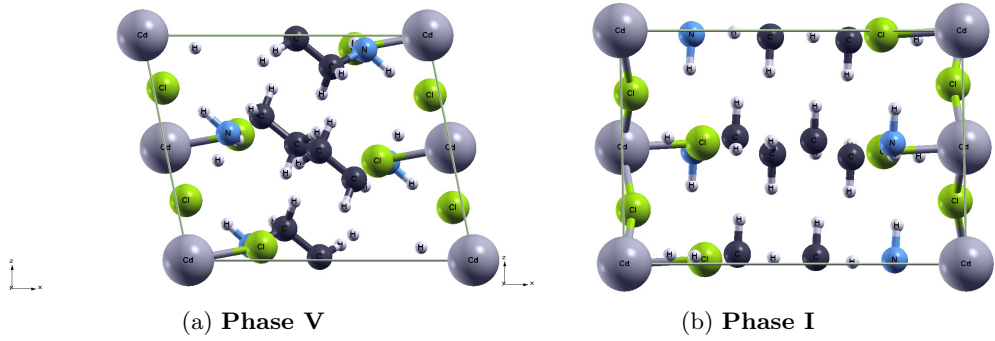


Fig. 1: Crystal structure of $[\text{NH}_3-(\text{CH}_2)_4-\text{NH}_3]\text{CdCl}_4$.

Table 1: Parameter of the two Phases of $[\text{NH}_3-(\text{CH}_2)_4-\text{NH}_3]\text{CdCl}_4$.

Crystal lattice Crystal- line system	Monoclinic Phase V : initial room-temperature form	Monoclinic Phase I : new room-temperature form
a	7.657 Å	7.344 Å
b	7.585 Å	7.485 Å
c	9.541 Å	10.775 Å
β	101.560°	91.060°
Z	2	2
Space group	$P2_1/a$	$P2_1/a$

GGA-PBE approach. The projected results between -12 eV and 12 eV are shown in Figure 2. The Fermi level is taken at the energy of 0 eV .

To obtain the precise band gap (see Table 2) of this compound, the generalized gradient approximation (GGA-PBE) was used.

Table 2: Gap energy values obtained by DFT+U method.

Crystal structure	$E_g(\text{eV})$	Fermi level (eV)	Gap type
Phase V	4.020	-0.463	indirect
Phase I	1.710	0.074	indirect

3.2.1 Case of the Phase V

Analysis of the density of states (DOS) plot (see Figures 2 and 3) pertaining to **Phase V** of $[\text{NH}_3-(\text{CH}_2)_4-\text{NH}_3]\text{CdCl}_4$ offers valuable insights into the orbital contributions of each constituent element (H, C, N, Cl, Cd) to the overall electronic configuration.

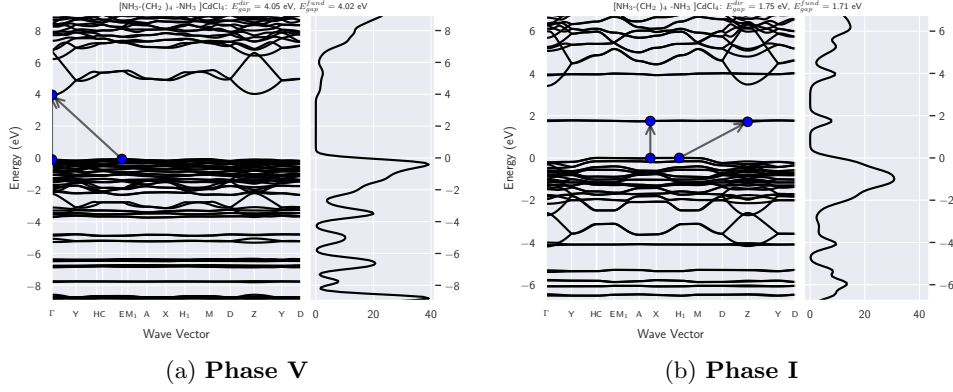


Fig. 2: Electronic band structures of $[\text{NH}_3-(\text{CH}_2)_4-\text{NH}_3]\text{CdCl}_4$.

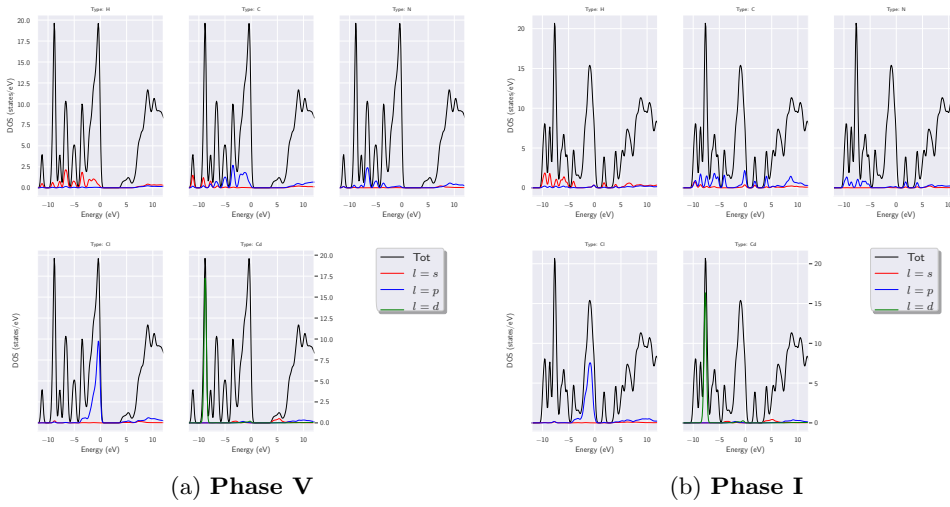


Fig. 3: Total and partial density of states of $[\text{NH}_3-(\text{CH}_2)_4-\text{NH}_3]\text{CdCl}_4$.

- Hydrogen (H): Examination of the DOS plot implies that the s -orbital plays a predominant role across the complete energy spectrum displayed, which is consistent with hydrogen's lone valence electron primarily occupying the s -orbital.
- Carbon (C): The primary contributor for carbon appears to be the p -orbital, exhibiting peaks throughout the spectrum, while the contribution from the s -orbital, if any, seems negligible compared to the p -orbitals. This observation indicates that carbon's four valence electrons predominantly reside in its p -orbitals.
- Nitrogen (N): Analogous to carbon, the dominant contributor for nitrogen seems to be the p -orbital, evident through peaks spanning the entire spectrum. The presence

of the s -orbital contribution, if existent, appears minor considering the scale, in accordance with nitrogen’s five valence electrons predominantly occupying its p -orbitals.

- Chlorine (Cl): Once again, the major contribution for chlorine is attributed to the p -orbital, with peaks distributed across the spectrum. The potential presence of the s -orbital contribution seems minor, reflecting chlorine’s seven valence electrons primarily filling its p -orbitals as indicated in the DOS plot.
- Cadmium (Cd): A significant contribution throughout the spectrum is observed from the d -orbital for cadmium, with the possibility of a presence of the p -orbital contribution, albeit weaker than the d -orbitals. The contribution from the s -orbital is anticipated to be minimal based on the scale, aligning with cadmium’s ten valence electrons occupying its $4d$ -orbitals and partially populating the $5p$ -orbitals.

The identification of a band gap (refer to Figure 3) ($E_g^{dir} = 4.050$ eV, $E_g^{fund} = 4.200$ eV) signifies the semiconductor nature of **Phase V** of $[\text{NH}_3-(\text{CH}_2)_4-\text{NH}_3]\text{CdCl}_4$. The wide band gap observed suggests potential utilization in optoelectronic devices designed for operation in the ultraviolet (UV) region.

In summary, the analysis of the DOS for the **Phase V** of $[\text{NH}_3-(\text{CH}_2)_4-\text{NH}_3]\text{CdCl}_4$ indicates a predominant role of p -orbitals for H, N, and Cl, with a substantial contribution from p -orbitals for carbon as well. Cadmium, characterized by filled d -orbitals, exhibits a significant contribution from d -orbitals to the DOS. The evaluation of the band gap validates the semiconductor characteristics of this phase, demonstrating a broad band gap and positioning it as a promising contender for UV optoelectronic applications.

3.2.2 Case of the Phase I

Like before (see Figures 2 and 3), the analysis of the partial density of states (PDOS) plot for the **Phase I** of $[\text{NH}_3-(\text{CH}_2)_4-\text{NH}_3]\text{CdCl}_4$ yields valuable insights into the orbital contributions of each constituent element to the total density of states (DOS).

- Hydrogen (H): Examination of the PDOS plot affirms the dominance of the s -orbital below the Fermi level with minimal contributions above it, consistent with the fact that hydrogen’s single valence electron primarily occupies the s -orbital. The marginal p -orbital contribution corresponds to expectations.
- Carbon (C): The p -orbital demonstrates significant contributions with notable peaks on either side of the Fermi level, while the s -orbital contribution is present but relatively smaller. This observation implies that carbon’s four valence electrons predominantly occupy its p -orbitals, although some involvement of s -orbitals is also evident.
- Nitrogen (N): Analogous to carbon, nitrogen exhibits a dominance of p -orbital contribution, with prominent peaks both below and above the Fermi level. The s -orbital contribution, although present, is comparatively minor, consistent with nitrogen’s five valence electrons primarily occupying its p -orbitals.

- Chlorine (Cl): Once again, the p -orbital manifests a significant contribution with peaks on both sides of the Fermi level, while the s -orbital contribution is minor. Chlorine’s seven valence electrons primarily occupy its p -orbitals, as indicated in the PDOS plot.
- Cadmium (Cd): Notably, the d -orbital displays a substantial contribution with significant peaks below and above the Fermi level. The p -orbital contribution is moderate, whereas the s -orbital contribution is minor, aligning with the presence of ten valence electrons in cadmium, occupying its $4d$ -orbitals and partially the $5p$ -orbitals.

The computed direct band gap ($E_g^{dir} = 1.750$ eV) and fundamental band gap ($E_g^{fund} = 1.710$ eV) deduced from the band structure plot indicate the semiconducting nature of the **Phase I** of $[\text{NH}_3-(\text{CH}_2)_4-\text{NH}_3]\text{CdCl}_4$. The presence of bands intersecting the Fermi level further substantiates the existence of electronic states in proximity to the band gap, potentially impacting electrical conductivity and other material properties.

In short, the examination of PDOS for the **Phase I** of $[\text{NH}_3-(\text{CH}_2)_4-\text{NH}_3]\text{CdCl}_4$ elucidates the pivotal role of p -orbitals in determining the DOS for H, N, and Cl. Carbon also exhibits a noteworthy contribution from p -orbitals, accompanied by some involvement of s -orbitals. Cadmium, characterized by filled d -orbitals, showcases a substantial contribution from d -orbitals to the DOS. The band gap analysis corroborates the semiconductor properties of the material. This profound comprehension of the electronic structure can offer valuable insights for customizing material properties for optoelectronic applications.

3.3 Optical properties

The study of the optical properties of solids has proven to be a powerful tool in understanding the electronic properties of materials. In this section, the study of optical properties is carried out using the GGA-PBE approximation, which has been shown to be successful in determining the optics band gap with appreciable precision. The optical properties of any material can be described by the complex dielectric function (see Equation (1)) [13]:

$$\varepsilon(\omega) = \varepsilon_1(\omega) + i\varepsilon_2(\omega). \quad (1)$$

It describes the optical response of the medium at all photon energies $E = \hbar\omega$. The real part of the dielectric function follows from the Kramers–Kronig relation (2) [13]:

$$\varepsilon_1(\omega) = 1 + \frac{2}{\pi} P \int_0^{\infty} \frac{\varepsilon_2(\alpha)}{\alpha^2 - \omega^2} \alpha d\alpha, \quad (2)$$

where P implies the principal value of the integral.

The imaginary part, $\varepsilon_2(\omega)$, in the long wavelength limit, has been obtained directly from the electronic structural calculation (see Equation (3)) [15]:

$$\varepsilon_2(\omega) = \frac{e^2 \hbar}{\pi m^2 \omega^2} \sum_{v,c} \int_{BZ} |M_{cv}(k)|^2 \delta[\omega_{cv}(k) - \omega] d^3k, \quad (3)$$

with $M_{cv}(k)$ the transition moment elements.

The following formula (4) is employed to calculate the absorption coefficient [13, 15, 16]:

$$\alpha(\omega) = \frac{\sqrt{2}}{c} \omega \sqrt{-\varepsilon_1(\omega) + \sqrt{(\varepsilon_1^2(\omega) + \varepsilon_2^2(\omega))}}. \quad (4)$$

The optical conductivity is given by the Equation (5) [11]:

$$\text{Re}(\sigma_{\alpha\beta}(\omega)) = \frac{\omega}{4\pi} \text{Im}(\varepsilon_{\alpha\beta}(\omega)). \quad (5)$$

The calculation of reflectivity is very important to evaluate the optical properties of materials; it makes it easy to understand the status and behavior of transparency, based on the reflectivity that we can draw from the transmittance. The reflectivity $R(\omega)$ (see Equation (6)) follows directly from the Fresnel's formula [15]:

$$R(\omega) = \left| \frac{\sqrt{\varepsilon(\omega)} - 1}{\sqrt{\varepsilon(\omega)} + 1} \right|^2. \quad (6)$$

It is also recommended to calculate the energy versus the wavelengths by varying the refractive index. This allows for an understanding of how the material can behave and how it can be canalized. To confirm the results found by the optical absorption and the transmittance, the refractive index $n(\omega)$ is given as follows in Equation (7) [13]:

$$n(\omega) = \sqrt{\frac{\sqrt{\varepsilon_1^2(\omega) + \varepsilon_2^2(\omega)} + \varepsilon_1(\omega)}{2}}. \quad (7)$$

This section presents a study of the effect of temperature on the optical properties of $[\text{NH}_3 - (\text{CH}_2)_4 - \text{NH}_3]\text{CdCl}_4$, including reflectivity and optical conductivity. Due to symmetry, the optical properties differ for the three directions, xx , yy and zz . The subsequent analysis will focus on the xx direction which is the most favorable for light production (the same consideration is also made for subsection 3.4).

It is well established that the imaginary part of the dielectric function $\varepsilon_2(\omega)$ is closely related to the electronic band structure and exhibits light absorption in the material [17]. Conversely, the real part of the dielectric function $\varepsilon_1(\omega)$ refers to the dispersion of the incident photons by crystals [18] and provides information regarding polarization [19]. The calculated static dielectric constants $\varepsilon_1(\omega)$ are equal to 121.046 0, and 55.535 9 for **Phase V** and **Phase I** of the compound, respectively (see Figures 4 g, h). As shown by the results, $\varepsilon_1(\omega)$ reaches a maximum at 0.002 7 eV for **Phase V**. For **Phase I**, $\varepsilon_1(\omega)$ reaches a maximum at 0.117 0 eV, then decreases and becomes

negative reaching a minimum at 0.1905 eV. Figures 4 i, j show a good correspondence between the imaginary part $\varepsilon_2(\omega)$ and the absorption peaks. For **Phase I**, the dielectric function increases sharply after 7 eV and 8 eV, giving the absorption edge. This threshold value comes mainly from the electronic transitions between the maxima of the valence band and the minima of the forbidden conduction band. Usually, it refers to the energy of the forbidden band, which agrees with the total density of this Phase. This result indicates that there is a reduction in the band gap, which is in agreement with the results found in electronic properties (Table 2).

Among the essential properties for photovoltaic applications is the reflectivity and the capacity of a sample surface to reflect incident radiation flux. Figures 4 c, d illustrate that reflectivity $R(\omega)$ decreases with an increase in wavelength, with the highest value of reflectivity which is 12 for **Phase V** and 8 for **Phase I**.

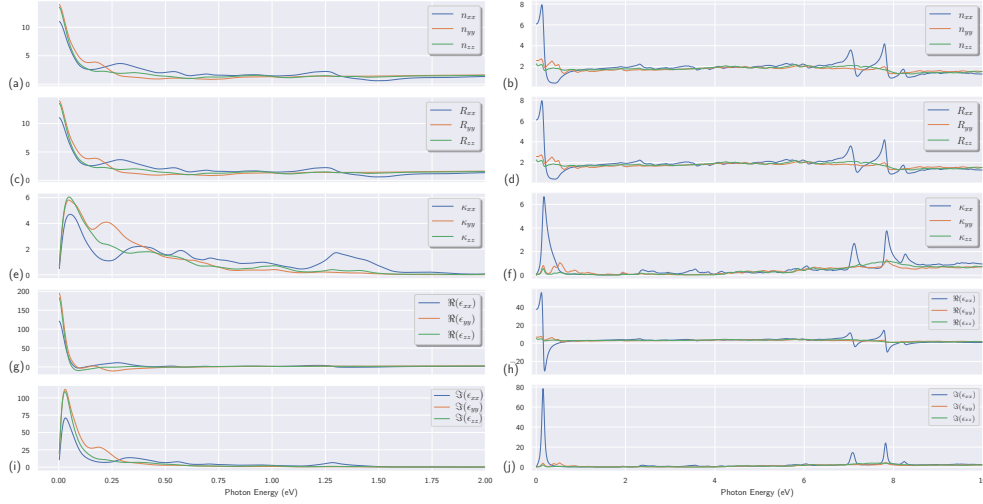


Fig. 4: Optical properties of $[\text{NH}_3 - (\text{CH}_2)_4 - \text{NH}_3]\text{CdCl}_4$. The left panel displays the optical properties of **Phase V**, while the right panel presents the optical properties of **Phase I**. Subplots (a) and (b) illustrate the reflective indexes, (c) and (d) depict the refractivities, (e) and (f) demonstrate the extinction coefficient k , (g) and (h) present the real part of the dielectric function, and (i) and (j) illustrate the imaginary part of the dielectric function.

The extinction coefficient for the xx direction is described in Figures 4 e, f. They demonstrate that the extinction coefficient is high at low photon energies and decreases as the energy increases. The values of the peaks for **Phase V** are 4.7013, 2.2148, 1.8937 and 1.7215 at an energy range of 0 to 1.7 eV, indicating specific absorption bands. While the peaks for **Phase I** are 6.6514, 2.6889, 3.7611 and 1.7846 at an energy range of 0 to 8.5 eV. A high extinction coefficient at low photon energies indicates significant absorption, which corresponds to electronic transitions or interband

absorption. Additionally, these peaks represent resonant absorption where the material absorbs light more effectively at specific energies.

These results indicate that $[\text{NH}_3-(\text{CH}_2)_4-\text{NH}_3]\text{CdCl}_4$ exhibits strong interaction with light at low photon energies, with high refractive indices, high reflectivity, and significant absorption. As the photon energy increases, these optical properties indicate reduced interaction, with lower refractive indices, lower reflectivity, and reduced absorption. These properties are consistent with typical dielectric materials, showing strong responses at lower energies and stabilizing at higher energies, making them potentially useful in applications where strong light interaction at low energies is desired, such as in optical coatings, sensors, or devices that require high refractive indices and strong absorption. The decrease in these properties at higher energies suggests good transparency and reduced reflection, which is beneficial for optoelectronic applications.

3.4 Thermoelectric properties

We have employed BoltzTrap2 software [20] to obtain thermo-electric properties of the two phases (**Phase V** and **Phase I**) of $[\text{NH}_3-(\text{CH}_2)_4-\text{NH}_3]\text{CdCl}_4$ with a constant relaxation time τ_0 . In order to ascertain the thermoelectric (TE) behaviour of both **Phase V** and **Phase I** in detail, the following characteristics have been expressed as a function of chemical potential: the Seebeck coefficient (S), electrical conductivity (σ), power factor (PF), electronic specific heat (Cv), electronic thermal conductivity (κ), number of concentration carriers (n) and density of states (DOS). The calculated characteristics have been plotted for a range of temperatures between 200 and 600 K.

The thermoelectric properties of any material are determined by its figure of merit, which is expressed as Equation (8):

$$ZT = \frac{1}{\kappa}(S^2\sigma T), \quad (8)$$

where:

- the Seebeck coefficient, which is a measure of a material's ability to generate a voltage difference from a temperature difference, is represented by the symbol S ,
- the symbol σ represents electrical conductivity,
- the symbol κ represents the thermal conductivity,
- the symbol T represents the absolute temperature.

As overall thermal conductivity increases, the figure of merit decreases, and S increases. A ZT value of at least one is often considered a benchmark for thermoelectric materials because it signifies that the material has favorable electrical and thermal properties for efficient energy conversion. Achieving a ZT greater than one is even more desirable, indicating higher efficiency. Furthermore, a material with a high ZT value is capable of achieving the optimal energy transformation efficiency, which is typically above 25 % at the optimal operating temperature [21].

In Figure 5 b, the electric conductivity as a function of chemical potential at room temperature first increases for both phases. It reaches its global maximum value.

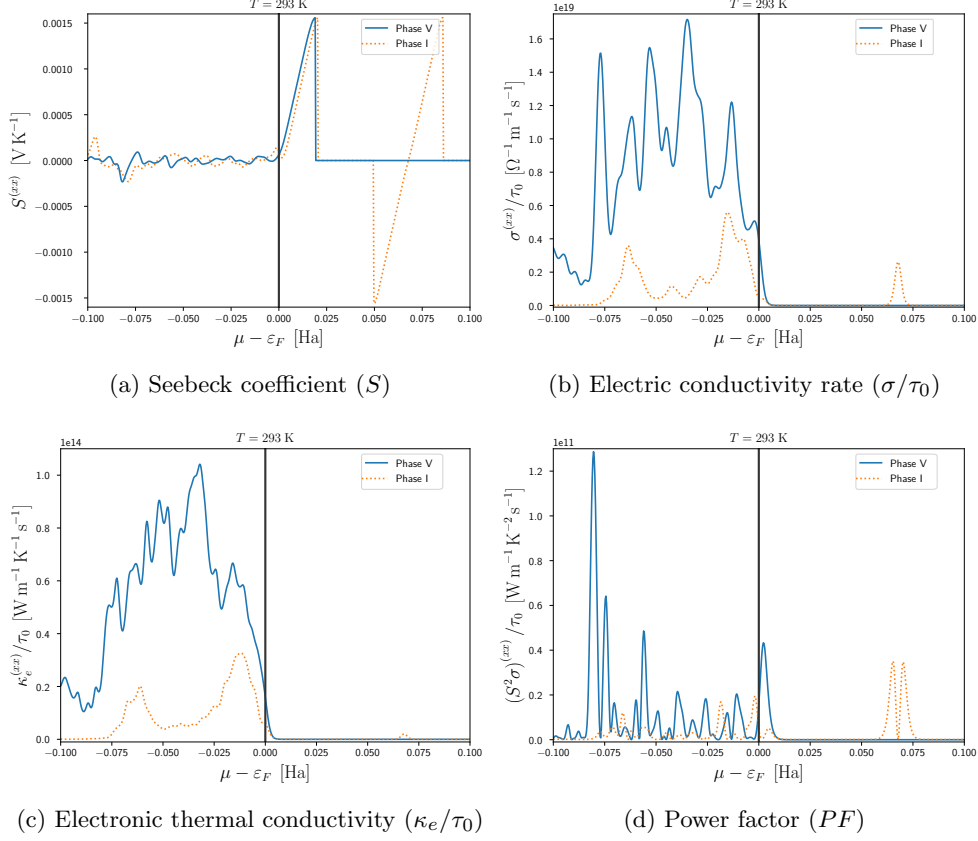


Fig. 5: Transition coefficients as a function of different ground state chemical potential at room temperature for the **Phase V** (blue line) and **Phase I** (dotted orange line) compounds.

Then it decreases and reaches its global minimum after the null value of the chemical potential at $\mu - \varepsilon_F = 0.0193$ Ha for **Phase V** and $\mu - \varepsilon_F = 0.0206$ Ha for **Phase I**.

The Figure 5 c displays the electronic thermal conductivity as a function of chemical potential. The behavior of the electronic thermal conductivity curves is nonlinear increasing for both compounds. The maximal electronic thermal conductivity of **Phase V** at RT is equal to $1.0416 \times 10^{14} \text{ W m}^{-1} \text{ K}^{-1}$, while it is $0.3264 \times 10^{14} \text{ W m}^{-1} \text{ K}^{-1}$ for **Phase I**.

The Figure 5 d shows how the power factor (PF) curves changed when the chemical potential increased for both compounds. They reach their maximum values of $1.2868 \times 10^{11} \text{ W m}^{-1} \text{ K}^{-2} \text{ s}^{-1}$ for **Phase V** and $0.3249 \times 10^{11} \text{ W m}^{-1} \text{ K}^{-2} \text{ s}^{-1}$ for **Phase I**. The findings indicate that the compound in **Phase V** exhibits superior performance compared to the compound in **Phase I**, contingent upon the utilization of an appropriate element dopant at specified concentrations and/or through band

engineering or transition to nanostructures. It is feasible to synthesize perovskite at the nanoscale, as evidenced by the reduction in lattice thermal conductivity. This will enhance the augmentation of thermoelectric efficiency.

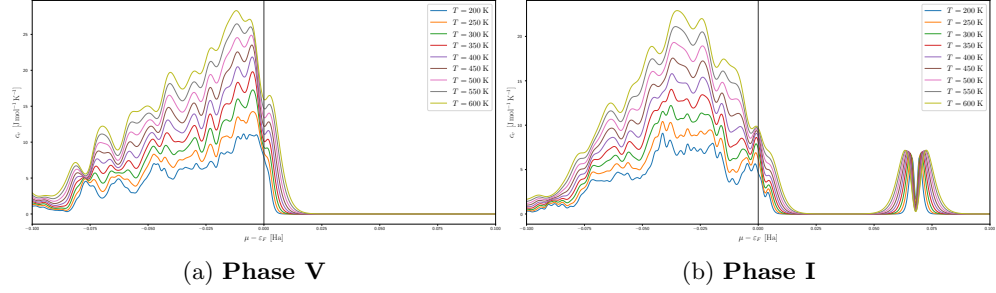


Fig. 6: The electronic specific heat as a function of chemical potential at different temperatures.

Figure 6 illustrates the electronic-specific heat capacity as a function of chemical potential at different temperatures. The calculated maximum value of the specific heat capacity of **Phase V** in this study is $16.8842 \text{ J mol}^{-1} \text{ K}^{-1}$ and $11.9643 \text{ J mol}^{-1} \text{ K}^{-1}$ for **Phase I** at RT. The C_v values for **Phase V** are slightly greater than those of **Phase I**.

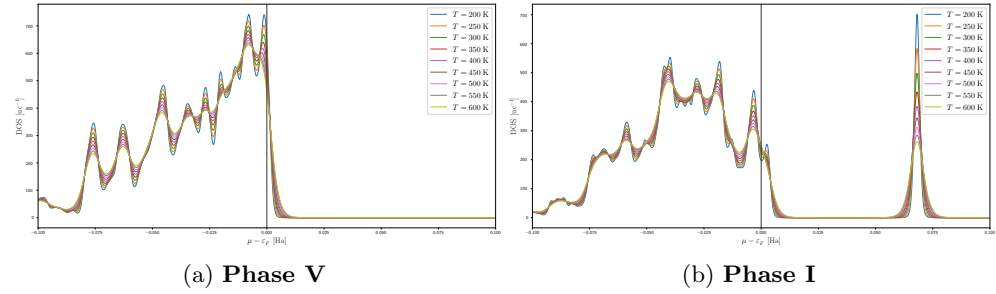


Fig. 7: The density of state at Fermi level DOS (uc^{-1}) as a function of chemical potential at different temperatures.

Figure 7 illustrates the variation in the density of the state around the Fermi level as a function of temperature. For the two alloys, **Phase V** and **Phase I**, the band gap persists over a wide range of temperatures.

Figure 8 presents the electrical conductivity in **Phase V** (left panel) and **Phase I** (right panel). In **Phase V**, the electrical conductivity of $[\text{NH}_3-(\text{CH}_2)_4-\text{NH}_3]\text{CdCl}_4$ exhibits multiple peaks at different temperatures. These peaks suggest changes in conductivity associated with Phase transitions or

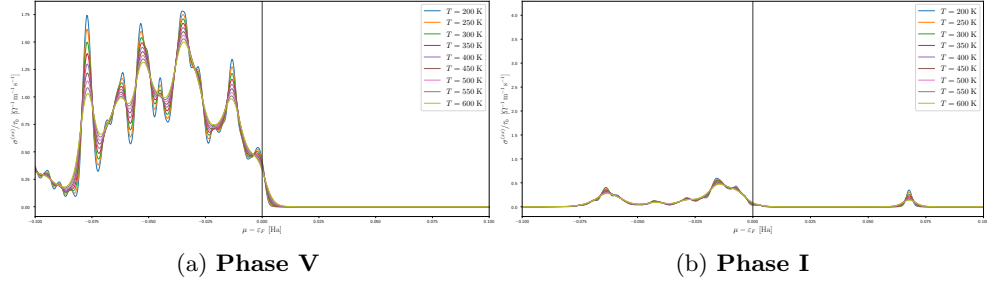


Fig. 8: Electrical conductivity rate (σ/τ) as a function of chemical potential at different temperatures.

structural modifications. The complex behavior likely arises from interactions between the $[\text{CdCl}_4]^{2-}$ anions and the organic cations $[\text{NH}_3-(\text{CH}_2)_4-\text{NH}_3]^{2+}$. In **Phase I**, there is a single prominent peak in the electrical conductivity which means that the overall conductivity is significantly lower compared to **Phase V**. This finding indicates that **Phase I** has different conductive properties, due to a distinct arrangement of ions and altered crystal structure caused by the effect of temperature. Structural Considerations like the structural dynamics of $[\text{NH}_3-(\text{CH}_2)_4-\text{NH}_3]\text{CdCl}_4$ likely play a crucial role in determining its electrical behavior. And Changes in hydrogen bonding (such as N-H-Cl interactions) and the arrangement of $[\text{CdCl}_4]^{2-}$ anions contribute to the observed conductivity variations.

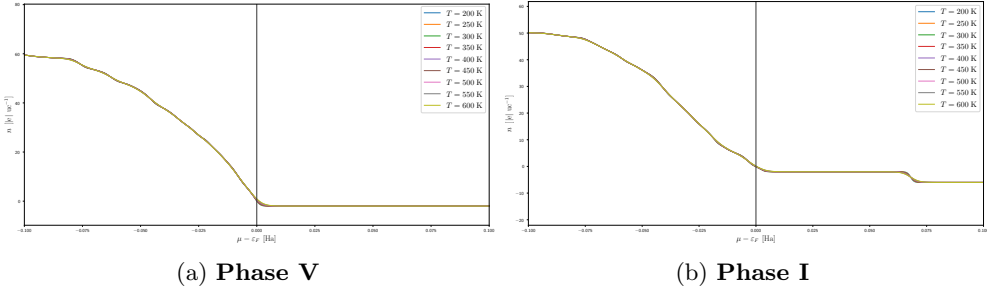


Fig. 9: Number of carrier concentration as a function of chemical potential at different temperatures. The efficiency of a thermoelectric device (n) is not determined by maximum ZT at a single temperature but depends on the average ZT over a wide temperature range following.

Figure 9 illustrates the carrier concentration in the two phases. The carrier concentration for both phases appears to be relatively constant across the distance measured. The carrier concentration for **Phase I** is slightly higher than that of **Phase V**. As is well known, the carrier concentration is typically used to refer to the number of charge carriers per unit volume in a semiconductor. In this context, a charge carrier could

be an electron or a hole. The results demonstrate that the temperature at which the measurement is taken affects the carrier concentration.

4 Conclusion

This inquiry, utilizing Density Functional Theory (DFT) computations, has thoroughly investigated the structural, electronic, optical, and thermoelectric attributes of the hybrid organic-inorganic perovskite $[\text{NH}_3-(\text{CH}_2)_4-\text{NH}_3]\text{CdCl}_4$ in its **Phase V** and **Phase I** configurations. Our results emphasize the considerable impact of phase transitions on the inherent characteristics of this material.

Structural optimization employing GGA-PBE produced lattice parameters in remarkable concordance with experimental observations, corroborating the validity of our computational methodology. A notable decrease in the band gap energy from 4.020 eV in **Phase V** to 1.710 eV in **Phase I** was detected, signifying enhanced electronic conductivity. Optical properties assessment disclosed augmented light absorption and interaction, particularly in **Phase I**, implying its potential for photovoltaic applications. Evaluation of thermoelectric properties illustrated the superior performance of **Phase V**, rendering it a promising candidate for thermoelectric devices. The distinct electrical conductivity profiles of the two phases highlight the effect of structural dynamics and temperature on the material's conductive behavior.

In summary, the observed variability in electronic and optical properties across the phases of $[\text{NH}_3-(\text{CH}_2)_4-\text{NH}_3]\text{CdCl}_4$ establishes this compound as a multifaceted material for optoelectronic and thermoelectric applications. Future inquiries could concentrate on investigating doping strategies and nanoscale synthesis to further enhance its properties.

Acknowledgements. This research was supported through computational resources of HPC-MARWAN (hpc.marwan.ma) provided by the National Center for Scientific and Technical Research (CNRST), Rabat, Morocco.

Declarations

- Conflict of interest/Competing interests: On behalf of all authors, the corresponding author states that there is no conflict of interest.
- Data availability: Data sets generated during the current study are available from the corresponding author on reasonable request.
- Code availability: Code used during the current study are available from the corresponding author on reasonable request.
- Author contribution: All authors contributed to the study conception and design. Code preparation, data collection and analysis were performed by Hafida ZIOUANI and Jean-Pierre TCHAPET NJAFA. The first draft of the manuscript was written by Hafida ZIOUANI and all authors commented on previous versions of the manuscript. All authors read and approved the final manuscript.

References

- [1] Borriello, I., Cantele, G., Ninno, D.: Ab initio investigation of hybrid organic-inorganic perovskites based on tin halides. *Physical Review B* **77**(23), 235214 (2008) <https://doi.org/10.1103/PhysRevB.77.235214>
- [2] Zhang, X., Zhao, L.-D.: Thermoelectric materials: Energy conversion between heat and electricity. *Journal of Materiomics* **1**(2), 92–105 (2015)
- [3] Hu, S., Ren, Z., Djurišić, A., Rogach, A.: Metal halide perovskites as emerging thermoelectric materials. *ACS Energy Letters* **6**(11), 3882–3905 (2021) <https://doi.org/10.1021/acsenergylett.1c02015>
- [4] Nyayban, A., Panda, S., Chowdhury, A.: Structural, electronic and optical properties of lead free rb based triiodide for photovoltaic application: an ab initio study. *Journal of Physics: Condensed Matter* **33**(37), 375702 (2021) <https://doi.org/10.1088/1361-648X/ac101b>
- [5] Khechoubi, M., Bendani, A., Chanh, N.B., Courseille, C., Duplessix, R., Couzi, M.: Thermal conformational changes in a bidimensional molecular composite material: A thermodynamic and crystallographic study of $\text{nh}_3\text{-(ch}_2\text{)}_4\text{-nh}_3\text{cdcl}_4$. *Journal of Physics and Chemistry of Solids* **55**(11), 1277–1288 (1994) [https://doi.org/10.1016/0022-3697\(94\)90210-0](https://doi.org/10.1016/0022-3697(94)90210-0)
- [6] Reiss, G.J.: Bis[(dimethylphosphoryl)methanaminium] tetrachloridopalladate(ii). *Acta Crystallographica Section E* **69**(11), 614–615 (2013) <https://doi.org/10.1107/S1600536813028067>
- [7] Ziouani, H., Mazouar, S., Tchapet Njafa, J.-P., Abdelilah, T., Ettakni, M., Khechoubi, E.M.: Structural and electronic properties of hybrid organic inorganic perovskite $[\text{nh}_3\text{-(ch}_2\text{)}_4\text{-nh}_3]\text{mcl}_4$ compound with ($m = \text{cu, mn, cd}$): Ab initio calculations. In: Elkhatabi, E.M., Boutahir, M., Termentzidis, K., Nakamura, K., Rahmani, A. (eds.) *Advanced Materials for Sustainable Energy and Engineering*, pp. 265–273. Springer, Cham (2024)
- [8] Gonze, X., Beuken, J.-M., Caracas, R., Detraux, F., Fuchs, M., Rignanese, G.-M., Sindic, L., Verstraete, M., Zerah, G., Jollet, F., Torrent, M., Roy, A., Mikami, M., Ghosez, P., Raty, J.-Y., Allan, D.C.: First-principles computation of material properties: The ABINIT software project. *Computational Materials Science* **25**(3), 478–492 (2002) [https://doi.org/10.1016/s0927-0256\(02\)00325-7](https://doi.org/10.1016/s0927-0256(02)00325-7)
- [9] Gonze, X., Rignanese, G.-M., Verstraete, M., Beuken, J.-M., Pouillon, Y., Caracas, R., Jollet, F., Torrent, M., Zerah, G., Mikami, M., Ghosez, P., Veithen, M., Raty, J.-Y., Olevano, V., Bruneval, F., Reining, L., Godby, R., Onida, G., D.C. Allan, D.R.H.: A brief introduction to the ABINIT software package. *Zeitschrift für Kristallographie - Crystalline Materials* **220**(5/6), 558–562 (2005) <https://doi.org/10.1524/zkri.220.5.558.65066>

- [10] Liechtenstein, A.I., Anisimov, V.I., Zaanen, J.: Density-functional theory and strong interactions: Orbital ordering in mott-hubbard insulators. *Phys. Rev. B* **52**(8), 5467–5470 (1995) <https://doi.org/10.1103/physrevb.52.r5467>
- [11] Perdew, J.P., Burke, K., Ernzerhof, M.: Generalized gradient approximation made simple [Phys. rev. lett. 77, 3865 (1996)]. *Phys. Rev. Lett.* **78**(7), 1396–1396 (1997) <https://doi.org/10.1103/physrevlett.78.1396>
- [12] Holzwarth, N.A.W., Tackett, A.R., Matthews, G.E.: A projector augmented wave (PAW) code for electronic structure calculations, part i: Atompaw for generating atom-centered functions. *Comput. Phys. Commun.* **135**(3), 329–347 (2001) [https://doi.org/10.1016/s0010-4655\(00\)00244-7](https://doi.org/10.1016/s0010-4655(00)00244-7)
- [13] Houmad, M., Zaari, H., Benyoussef, A., El Kenz, A., Ez-Zahraouy, H.: Optical conductivity enhancement and band gap opening with silicon doped graphene. *Carbon* **94**, 1021–1027 (2015) <https://doi.org/10.1016/j.carbon.2015.07.033>.
- [14] Murnaghan, F.D.: The compressibility of media under extreme pressures. *Proceedings of the National Academy of Sciences of the United States of America* **30**, 244–247 (1944) <https://doi.org/10.1073/pnas.30.9.244>
- [15] Khenata, R., Bouhemadou, A., Sahnoun, M., Reshak, A.H., Baltache, H., Rabah, M.: Elastic, electronic and optical properties of zns, znse and znTe under pressure. *Computational Materials Science* **38**(1), 29–38 (2006) <https://doi.org/10.1016/j.commatsci.2006.01.013>
- [16] Houmad, M., Dakir, O., Abbassi, A., Benyoussef, A., El Kenz, A., Ez-Zahraouy, H.: Optical properties of sic nanosheet. *Optik* **127**(4), 1867–1870 (2016) <https://doi.org/10.1016/j.ijleo.2015.11.017>
- [17] Rizwan, M., Ayub, A., Shakil, M., Usman, Z., Gillani, S.S.A., Jin, H.B., Cao, C.B.: Putting dft to trial: For the exploration to correlate structural, electronic and optical properties of m-doped (m = group i, ii, iii, xii, xvi) lead free high piezoelectric c-bialo₃. *Materials Science and Engineering: B* **264**, 114959 (2021) <https://doi.org/10.1016/j.mseb.2020.114959>
- [18] Absike, H., Labrim, H., Hartiti, B., Douhou, K., Ez-Zahraouy, H.: Ab initio calculations on electronic, optical, and thermoelectric properties of (si, pb) (co)-doped zns for solar cell device applications. *Journal of Physics and Chemistry of Solids* **132**, 10–17 (2019) <https://doi.org/10.1016/j.jpcs.2019.03.030>
- [19] Rizwan, M., Gul, S., Mahmood, T., Shakil, M., Majid, A., Rafique, M., Zafar, A.A., Jin, H.B., Cao, C.B.: Tailoring electronic and optical properties of laalo₃ by cu inclusion: a dft study. *Canadian Journal of Physics* **99**(1), 38–43 (2021) <https://doi.org/10.1139/cjp-2019-0558> <https://doi.org/10.1139/cjp-2019-0558>

- [20] Madsen, G.K.H., Carrete, J., Verstraete, M.J.: BoltzTraP2, a program for interpolating band structures and calculating semi-classical transport coefficients. *Comput. Phys. Commun.* **231**, 140–145 (2018) <https://doi.org/10.1016/j.cpc.2018.05.010>
- [21] Alrahamneh, M.J., Mousa, A.A., Khalifeh, J.M.: First principles study of the structural, electronic, magnetic and thermoelectric properties of zr2rhal. *Physica B: Condensed Matter* **552**, 227–235 (2019) <https://doi.org/10.1016/j.physb.2018.10.018>